Synergy between surface adsorption and photocatalysis during degradation of humic acid on TiO2/activated carbon composites

Gang Xue[a], Huanhuan Liu[a], Quanyuan Chen[a,*], Colin Hills[b], Mark Tyrer[c], Francis Innocent[a]

[a] School of Environmental Science and Engineering, Donghua University, 1884 Yian Road (West), Shanghai 200051, PR China
[b] Centre for Contaminated Land Remediation, School of Science, University of Greenwich, Chatham Maritime, Kent ME4 4TB, UK
[c] Centre for CO2 Technology, University College London, WC1E 7JE, UK

ARTICLE INFO

ABSTRACT

A photocatalyst comprising nano-sized TiO2 particles on granular activated carbon (GAC) was prepared by a sol-dipping–gel process. The TiO2/GAC composite was characterized by scanning electron microscopy (SEM), X-ray diffractometry (XRD) and nitrogen sorptometry, and its photocatalytic activity was studied through the degradation of humic acid (HA) in a quartz glass reactor. The factors influencing photocatalysis were investigated and the GAC was found to be an ideal substrate for nano-sized TiO2 immobilization. A 99.5% removal efficiency for HA from solution was achieved at an initial concentration of 15 mg/L in a period of 3 h. It was found that degradation of HA on the TiO2/GAC composite was facilitated by the synergistic relationship between surface adsorption characteristics and photocatalytic potential. The fitting of experimental results with the Langmuir–Hinshelwood (L–H) model showed that the reaction rate constant and the adsorption constant values were 0.1124 mg/(L min) and 0.3402 L/mg. The latter is 1.7 times of the calculated value by fitting the adsorption equilibrium data into the Langmuir equation.

© 2010 Elsevier B.V. All rights reserved.

1. Introduction

Humic acids (HAs) consist of a skeleton of alkyl/aromatic units cross-linked by a variety of functional groups such as carboxylic, phenolic and alcoholic hydroxyls, ketone and quinone groups [1,2]. The existence of carboxyl and phenolic groups causes humic acid to have negative charges in aqueous solutions. The solubility of humic acid in aqueous media also depends on the number of –COOH and –OH groups. Humic acids show spontaneous changes in their conformation and aggregation state as a function of solution conditions such as concentration, pH and ionic strength [2–4].

Humic acids are depicted as model compounds of natural organic matter (NOM) and are main precursors of disinfection by-products in potable water production, as humic acids can react with chlorine during water treatment producing carcinogenic substances, for example, trihalomethanes. Thus, the elimination of humic acids is required before the chlorination of drinking water, and the heterogeneous photocatalytic degradation has shown great potential for NOM removal [5–7].

Nano-sized TiO2 is one of the most efficient semiconductors currently available for the photocatalytic degradation of environmental pollutants [8]. Upon exposure to UV radiation, pre-adsorbed O2 and H2O molecules react on electron–hole pairs (e^-CB/h^+VB) that can migrate to the surface to form oxidizing species (e.g., $HO_2^\bullet$, $O_2^{\bullet-}$ and $OH^\bullet$ radicals). These radical species possess the potential to oxidize various organic molecules.

Nano-sized TiO2 photocatalysts have been used in a variety of reactor configurations including fluidized beds, immobilized films, circulating columns and membrane reactors [9–12], but their fineness prevents removed by sedimentation. An alternative, investigated here, is to immobilize nano-TiO2 particles onto a suitable coarse solid substrate to facilitate the practical application of the photocatalytic process.

Nano-sized TiO2 particles can be immobilized on ceramic, glass, plastic, and polyvinyl chloride-coated fabrics using many different techniques [13–17], but the efficient oxidation of organics requires adsorption onto the surface of TiO2 because the photocatalytic process is surface orientated [18]. As granular activated carbon (GAC) possesses a high surface area, high adsorption capacity and suitable pore structure, and nano-sized TiO2 facilitates photocatalysis, TiO2/GAC composite substrates are receiving increasing attention through the degradation of humic and phenolic compounds, pesticides, chlorinated compounds and dyes [19–30]. The decomposition of these contaminants with respect to the removal efficiency, reaction rate, and the formation of intermediates have also been investigated [31–33]. However, there is little experimental information available concerning the synergistic effects of adsorption and photocatalytic activity, and a thorough

* Corresponding author. Tel.: +86 021 6779 2540; fax: +86 021 6779 2552.
E-mail address: qychen@dhu.edu.cn (Q. Chen).

understanding of this relationship is important for the design and application of efficient TiO$_2$/GAC systems.

In the present work, nano-sized TiO$_2$ was immobilized on granular activated carbon (GAC) by a sol-dipping–gel process. The synergistic relationship between surface adsorption characteristics and photocatalytic potential was examined by the comparisons of typical reaction systems during the degradation of humic acid solutions.

2. Experimental

2.1. Preparation of the composite photocatalyst

The nano-sized TiO$_2$ coated granular activated carbon composite (TiO$_2$/GAC) was prepared by a sol-dipping–gel route, using tetra-*n*-butyl titanate as the precursor. During the preparation, 68.7 mL Ti (OC$_4$H$_9$)$_4$ (C.P., SCRC, China) was dissolved in 117 mL ethanol, and was stirred for 2 h (100 rpm) with a magnetic stirrer. Whilst still stirring, at an ambient laboratory temperature of 20 °C, a solution containing 3.33 mL HCl (35%) and 0.36 mL de-ionized water was added drop by drop over 1 h. Following this, 6.20 mL of acetyl acetone was slowly added to stabilize the sol. After aging for 24 h at the room temperature, the sol was mixed with activated carbon granules of 70–100 mesh (Shanghai Shenshui Water Treatment Equipment Plant) derived from nut kernels, that was washed with boiled de-ionized water prior to use. The sol-coated activated carbon was dried for 30 min at 105 °C in an oven and then calcined at temperature of 300 °C for 2 h in a nitrogen atmosphere. The dipping and calcining procedure was repeated up to 5 times, prior to the last cycle where the temperature, was held at 500 °C. Simultaneously, the aging gel was also calcined at 500 °C for 2 h to synthesize pure nano-sized TiO$_2$ powders for comparison.

2.2. Characterization of the composite photocatalyst

The profile of the TiO$_2$/GAC photocatalyst was observed by scanning electron microscopy (Hitachi X650, Japan) at an accelerating voltage of 10 kV.

X-ray diffraction (XRD) can provide valuable information about crystalline nature of the nano-sized TiO$_2$. In this work, diffractograms were obtained at room temperature with a D/Max-2550 PC diffractometer (Rigaku, Japan) with copper Kα radiation and the average crystal size of the TiO$_2$ powders was estimated by using Scherrer's formula:

$$D = \frac{0.89\lambda}{\beta(2\theta)\cos\theta} \tag{1}$$

where λ is the wavelength of the X-ray radiation ($\lambda = 0.15418$ nm), θ is X-ray diffraction angle and β is the full-width at half maximum (FWHM) of the (1 0 1) plane of TiO$_2$ (in radians), corrected for instrumental broadening ($\beta_0 = 0.00122$ rad) prior to calculation of the particle size broadening.

Nitrogen adsorption–desorption isotherms were used to determine BET surface area and pore size distribution (Micromeritics BELSORP-mini, Japan, BEL) at 77 K. Specific surface area was calculated from the BET isotherms and the pore size distribution was determined by the density functional theory (DFT) method [34].

The TiO$_2$/GAC composite was ignited at 900 °C and the TiO$_2$ loading amount was calculated by ash weight.

2.3. Feed water and chemicals

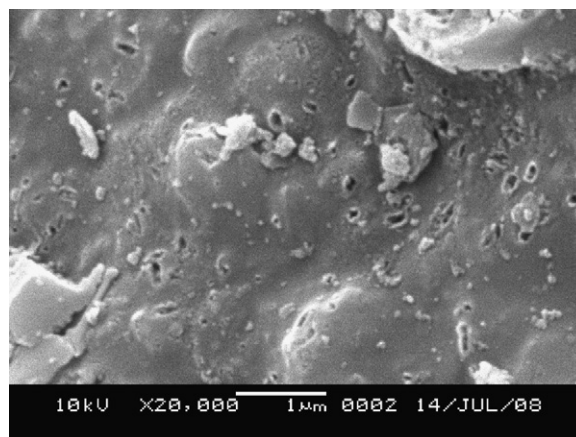A filtered (0.45 μm Millipore membrane) feed solution contained HA (Biochemical reagent, Shanghai Jufeng Chemicals)

Fig. 1. SEM image of the TiO$_2$/GAC composite photocatalyst.

dissolved in de-ionized water. It should be noted that HA is soluble in de-ionized water at pH 4–11, in concentrations of less than 100 mg/L.

The TOC was measured using a TOC analyzer (model 820, Sievers, USA), and the absorbance of solutions was determined using a TU-1810 UV/Vis Spectrophotometer (Beijing Puxi Instrument Co. Ltd.), calibrated at 254 nm.

2.4. The photocatalytic reactor

Experiments were carried out using a cylindrical batch reactor (8 cm in diameter and 12 cm in height) fitted with a 5 cm diameter water-cooled quartz jacket (XPA-II, Xujiang Mechanical Electronics, Nanjing), which maintained the temperature at 38 ± 1 °C.

2.5. Experimental procedure

The experimental procedure involved placing 500 mL of filtered solution (15 mg/L of HA, corresponding to a TOC of 5.04 mg/L) in the photocatalytic reactor. Dispersion was maintained by gentle continuous stirring (100 rpm) with a magnetic stirrer, whilst a high-pressure 500 W mercury lamp (major emission at 365 nm, 12.5 mW/cm^2) provided the intense light source. Air was bubbled through the reaction solution to ensure a constant dissolved oxygen concentration. Thereafter, 20 mL samples were collected at 30 min intervals and filtered (pre-washed 0.45 μm cellulose acetate membrane). The degradation of HA, UV$_{254}$ was measured in a 10 mm quartz cell in the TU-1810 spectrophotometer, as the concentration of HA in solution changes as degradation proceeded.

The dosage of TiO$_2$/GAC was 2 g/L and the initial pH values of HA solution were in the range of 7.2–7.5, unless otherwise specified. A HA control solution containing nano-sized TiO$_2$, maintained at 0.4 g/L, was also tested in triplicate and the results are reported as mean values, with an error of less than 5%.

3. Results and discussion

3.1. Pore structure of TiO$_2$/GAC

The TiO$_2$/GAC photocatalyst was gold-covered and examined with scanning electron microscopy. Fig. 1 illustrates the electron micrograph of the TiO$_2$/GAC composite photocatalyst. It is obvious that TiO$_2$ particles were well dispersed on the surface of GAC, and the particle size was in the range of nanometer scale. This was due to the high surface area of GAC matrix, which favored a high degree of dispersion of TiO$_2$ particles. Note that the TiO$_2$ particles as shown in the SEM picture were the agglomerates of many TiO$_2$ crystallites.
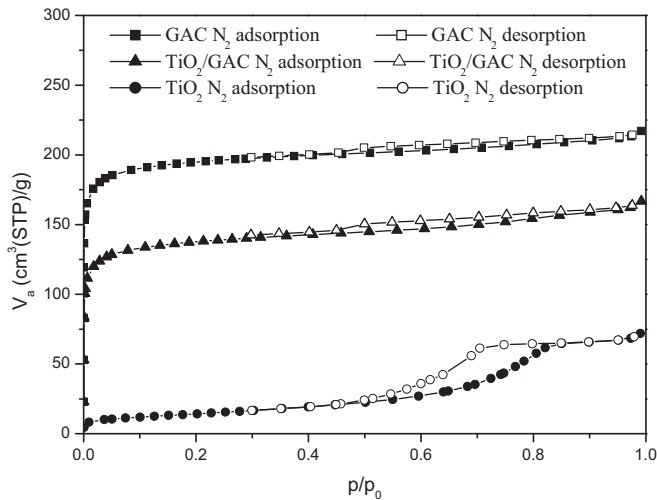
Fig. 2. Nitrogen adsorption isotherms for GAC, TiO$_2$ and TiO$_2$/GAC.

As expected, TiO$_2$ particles not only deposited on the surface, but also in the mesopores and macrospores of GAC. TiO$_2$ on the external surface will have more chances to receive light and exhibited higher catalytic activity.

The nitrogen adsorption isotherms for the TiO$_2$/GAC composite and TiO$_2$ powders and GAC (see Fig. 2) provided the pore characteristics summarized in Table 1. The BET surface area of TiO$_2$ powder, GAC and TiO$_2$/GAC was 52.16 m^2/g, 771.07 m^2/g and 536.82 m^2/g, respectively. The total pore and micro-pore volume of TiO$_2$/GAC were lower than those of GAC, indicating that some pores were covered or blocked by the TiO$_2$ film. The pore size distributions (Fig. 3) show a sharp peak at 0.6 nm and although the total surface area decreased after TiO$_2$ loading, most TiO$_2$ particles agglomerated on the outer surface of GAC, as two curves were very similar.

The adsorptive efficiency of TiO$_2$/GAC to HA was controlled by the pore diameter within the GAC, and molecular size of humic acid. The results from dynamic light scattering and voltammetry show that humic matter present in solution is aggregated in relatively large particles (>30 nm) and some irreversible disaggregation (120 nm diameter) is promoted by pH increase up to 10 [35–39]. The aggregates present in solution seem to be of a dynamic nature being influenced by changes of concentration, pH and/or ionic strength, although not always in the same way for samples of different origins and/or with different preparation procedures [2–4]. Humic matter, formed by polymer coils expanded at low ionic strength due to charge repulsion, tends to be coil-like if enough supporting electrolyte is added, which is reflected in the decrease of the hydrodynamic diameter of HAs when the ionic strength increases. If the pore diameter matches molecular size e.g. at ratio of 1.7, adsorption can occur on the internal surface of GAC [1]. It is likely that the HA molecules were adsorbed on the outer surface of the TiO$_2$/GAC composite and not into the micro-pores within TiO$_2$/GAC, which ranged from 0.5 nm to 1.0 nm (see Fig. 3). Powell and Town [37] observed in dialysis experiments that HA aggregates larger than the molar mass cut-off of the

Table 1
Pore characteristics of GAC, TiO$_2$ and TiO$_2$/GAC.

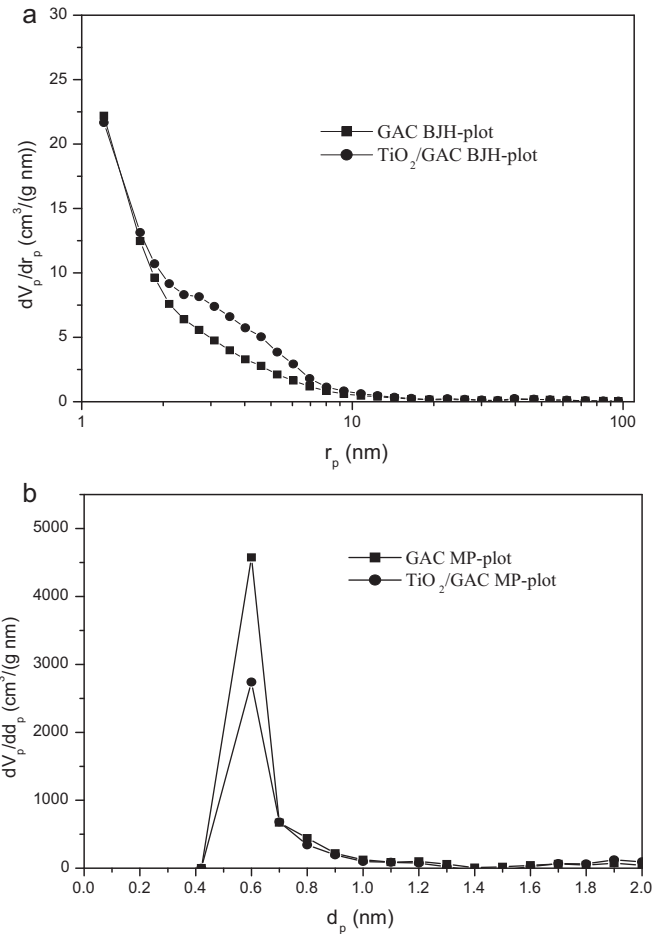| Sample	BET specific surface area (m^2/g)	Total pore volume (cm^3/g)	Micro-pore volume (cm^3/g)	Average pore size (nm)
GAC	771.07	0.3351	0.3288	1.7362
TiO$_2$/GAC	536.82	0.2571	0.2272	1.9155
TiO$_2$ powders	52.16	–	–	–

Fig. 3. Pore distribution for GAC and TiO$_2$/GAC ((a) BJH plot of pores and (b) MP plot of pores).

membrane were found in the dialysed solution. This suggest that a humic aggregate could partially disaggregate, crossing the membrane and re-aggregate on the other side. If such a phenomenon is real then a few small humic acid molecules may enter to micro-pores of TiO$_2$/GAC photocatalyst used.

The amount of TiO$_2$ immobilized and the specific surface area of TiO$_2$/GAC (Fig. 4) showed that as the amount increased, the specific surface area decreased, as some surface pores became occluded, by the TiO$_2$ particles.
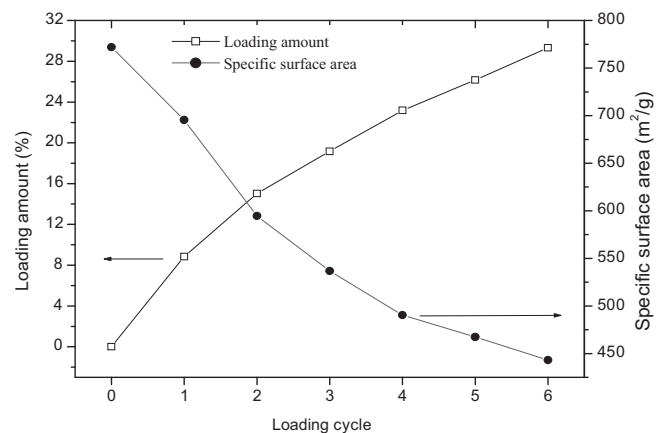

Fig. 4. The influence of loading cycles on the TiO$_2$ immobilized amount and the specific surface area of TiO$_2$/GAC.
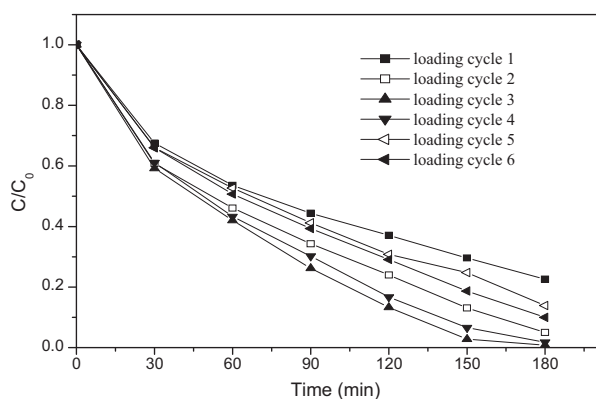
Fig. 5. The influence of cyclic TiO$_2$ loading on the photocatalytic activity.

The relationship between TiO$_2$ loading-cycle on photocatalytic activity is shown in Fig. 5. The removal of HA from the 1, 2, 3, 4, 5, and 6 loading cycles were 78%, 95%, 99%, 98%, 86% and 90%, respectively, showing that photocatalytic activity of the substrate declined slightly above 4 cycles despite increasing TiO$_2$ loading (see Fig. 4). The existence of an optimal loading indicated that loading and BET surface area are two mutually constrained factors influencing photocatalytic efficiency.

3.2. Influence of calcination temperature

At a TiO$_2$/GAC dose of 2 g/L, the temperature of the final cycle of photocatalyst calcination on HA degradation was important (see Fig. 6). The 99.5% removal of HA coincided with a final calcination temperature of 500 °C. According to the literature (e.g., [8]), higher temperatures will result in greater rutile formation and increase TiO$_2$ particle size and agglomeration; and a coincident reduction in photocatalytic activity. The mass loss of activated carbon was also important as at 500 °C it was 8%, whereas at 600 °C this loss increased dramatically to 54.7%.

Examination by XRD showed that anatase was formed at a temperature of 500 °C (see Fig. 7 and Table 2). A comparison of the TiO$_2$/GAC composite photocatalyst and TiO$_2$ powders, showed differences in TiO$_2$ crystallinity and particle size, with the latter calculated using Scherrer's formula for the main peak (25°2θ) as 11.7 nm and 12.3 nm, respectively.
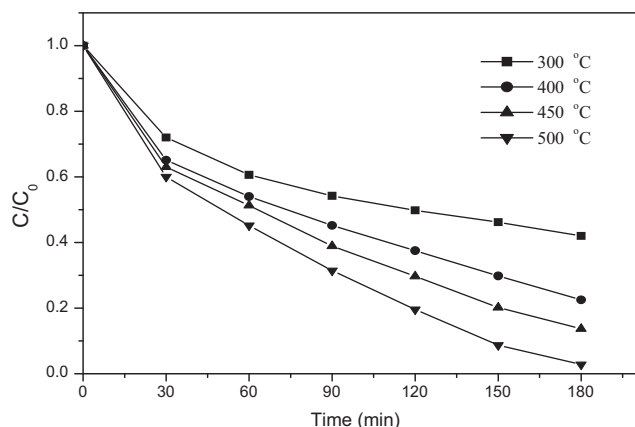

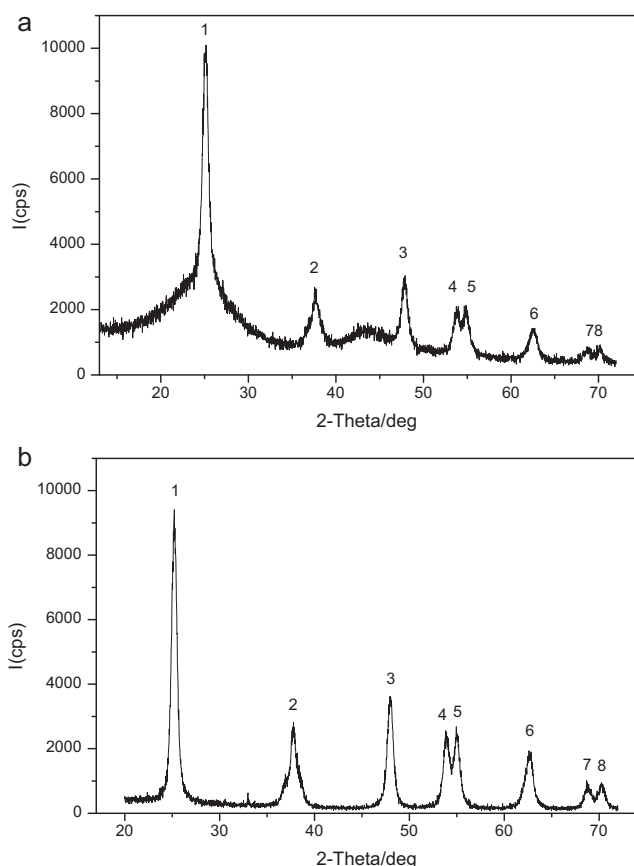**Fig. 6.** Effects of photocatalyst calcination temperature on HA degradation.

Fig. 7. Diffractograms obtained from (a) TiO$_2$/GAC and (b) TiO$_2$.

3.3. Influence of pH

HA is soluble in alkaline solution to weakly acidic solutions, but deposits at or below pH 2.0. The photocatalytic degradation of HA increased as pH decreased (Fig. 8). Usually, TiO$_2$ shows a higher photocatalytic activity under acidic conditions. That is because the positively charged catalyst surface is conducive to the transferring process of photogenerated electrons to the surface of catalyst, which contributes to the generation of active radicals such as O$_2^{\bullet-}$ and OH$^{\bullet}$ in the presence of oxygen in aqueous medium, and meanwhile avoids the recombination of photogenerated electrons and holes. This phenomenon can also be attributed to the reduction of HA adsorption on the surface of TiO$_2$/GAC. As is well known, macromolecules of humic acid contain conjugated olefinic, aromatic, phenolic–semiquinone–quinone structures of a wide spectrum with functional groups (–CO, –COOH, –OH, –NH–, –NH$_2$, –N–), whereas GAC possesses a well-developed pore structure with large surface area and large numbers of active adsorption sites. However, at high pH's humic acid cannot adsorb onto the negatively charged TiO$_2$/GAC surface. This lowered the photocatalytic degradation of HA at high pH, as adsorption of reacting substances onto the surface of the catalyst is an important step in the photocatalytic process. According to the literature [37–39], HAs, initially set to pH 10 and then adjusted to pH between 3 and 5, present somehow different characteristics from samples directly set to the required pH. The differences observed may also be associated with the possibility that humic acids may aggregate to the extent of forming micelle-like structures [36,37]. The results in Fig. 8 may suggest that photocatalytical degradation of humic acids is relative to their conformation and aggregation state.

Table 2
Comparison of X-ray diffraction peaks ($2\theta/°$).

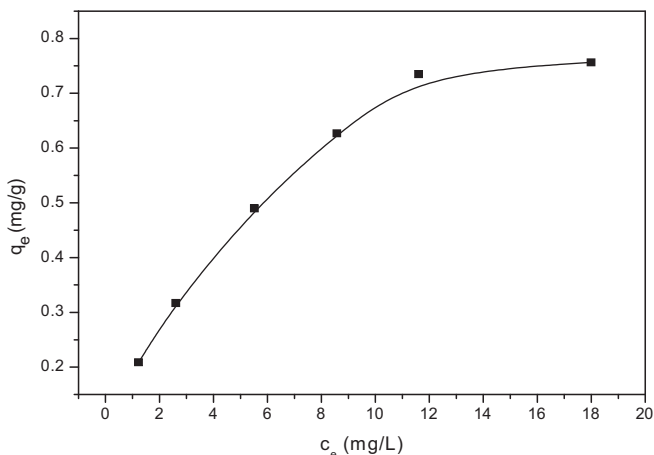|	Peaks							
	1	2	3	4	5	6	7	8
TiO$_2$/GAC	25.16	37.62	47.78	53.84	54.90	62.66	68.72	70.22
TiO$_2$ powders	25.18	37.80	48.00	53.84	54.98	62.64	68.72	70.24
Anatase (PDF 21-1272)	25.28 (1 0 1)	37.80 (0 0 4)	48.05 (2 0 0)	53.89 (1 0 5)	55.06 (2 1 1)	62.69 (2 0 4)	68.76 (1 1 6)	70.31 (2 2 0)
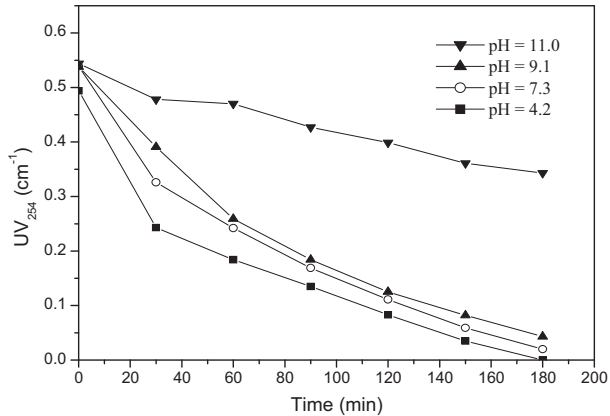
Fig. 8. The influence of pH on HA degradation at TiO$_2$/GAC dosage of 2 g/L.

3.4. Synergy between adsorption and photocatalytic degradation

The adsorption of humic acid onto TiO$_2$/GAC is dependent upon the surface charge, hydrophobicity, and pore structure of the substrate and solution conditions. The amount of HA adsorbed at its equilibrium concentration without UV light over 30 min (see Fig. 9) was measured and fitted to the Langmuir and Freudlich equations. The Langmuir isotherm constants were obtained from the plot of $1/q_e$ against $1/C_e$:

$$\frac{1}{q_e} = \frac{1}{q_{max}} + \frac{1}{q_{max}bC_e} \tag{2}$$

where q_{max} (mg/g) is adsorption capacity and b is a constant related to the affinity of the binding sites (L/mg); q_e (mg/g) and C_e (mg/L) are the amount of HA adsorbed per unit mass of TiO$_2$/GAC, and the un-adsorbed HA concentration in solution at equilibrium, respectively. The Freundlich constants were be obtained from the plot of lg q_e

Table 3
Adsorption constants for humic acid on the surface of TiO$_2$/GAC.

Langmuir			Frendich		
R^2	b (L/mg)	q_m (mg/g)	R^2	K_F (mg/(g(L/mg)$^{1/n}$))	$1/n$
0.9946	0.1992		0.9877	0.9892	0.1963	0.5104

against lg C_e:

$$lg\, q_e = \frac{1}{n} lg\, C_e + lg\, K_F \tag{3}$$

where C_e is the equilibrium concentration of HA (mg/L); q_e is the amount of HA adsorbed per unit mass of adsorbent (mg/g); K_F (mg/g$(L/mg)^{1/n}$) and n (dimensionless) signifies the adsorption capacity and adsorption intensity respectively. The slope of $1/n$ ranging between 0 and 1 is a measure of surface heterogeneity, with the surface becoming more heterogeneous as its value gets closer to zero.

The linear fitted curves obtained from the HA sorption isotherms are given in Table 3, and the constant related to the affinity of the binding sites (b) is a 0.1992 L/mg and adsorption intensity ($1/n$) is 0.5104, implying that the distribution of TiO$_2$ on the surface of GAC is even.

The kinetics of HA adsorption on TiO$_2$/GAC (Fig. 10) can be fitted into the pseudo second-order Lagergren equation:

$$\frac{dq}{dt} = K_2(q_e - q)^2 \tag{4}$$

or:

$$\frac{t}{q} = \frac{1}{K_2 q_e^2} + \frac{1}{q_e}t \tag{5}$$

where q_e is the amount of HA adsorbed per unit mass of adsorbent (mg/g); q is the amount of HA adsorbed per unit mass of adsorbent at different time (mg/g); and K_2 is the adsorption constant (g/mg min).

The fitted parameters to the pseudo second-order Lagergren equation are presented in Table 4. The very high R^2 values of

Fig. 9. Adsorption isotherms for humic acid on the surface of TiO$_2$/GAC.
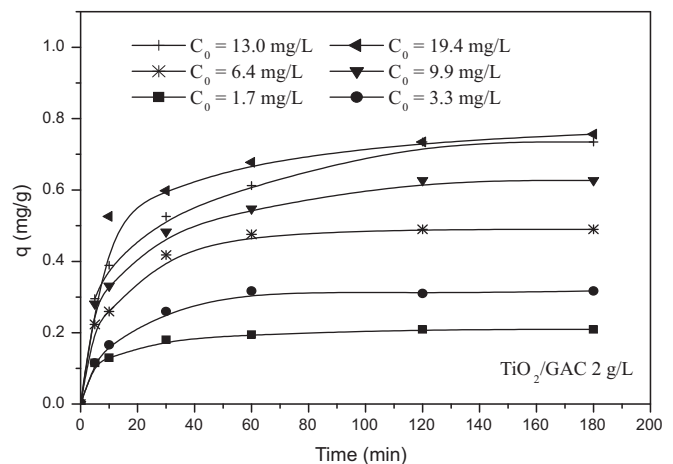
**Fig. 10.** Kinetics of HA adsorption on the surface of TiO$_2$/GAC.

Table 4
The fitted parameters of adsorption kinetics using the pseudo second-order Lagergren equation.

|	HA initial concentration (mg/L)				
	1.7	3.3	6.4	9.9	13.0
R^2	0.9992	0.9972	0.9984	0.9976	0.9948
K_2	0.8076	0.3636	0.2777	0.1571	0.1092

0.9992–0.9948 shows that it is appropriate to consider that the adsorption of HA was controlled by the adsorption mechanism and not controlled by diffusion or mass transfer inside the substrate particles. This is in agreement with the inference above base on the pore size.

In the aqueous TiO_2/GAC–HA suspension, the contribution from adsorption, photo-degradation and photocatalytic degradation was important, as shown in Fig. 11, where "photo-degradation" means photolysis of HA under the UV light only, without TiO_2/GAC in the solution, whilst "photocatalytic degradation" means degradation of HA under the UV light using TiO_2/GAC as a photocatalyst in the solution.
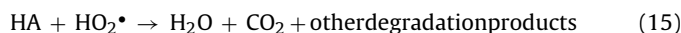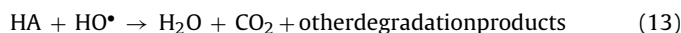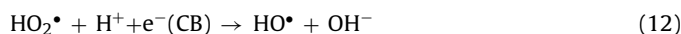
Under UV illumination, TiO_2 particles on GAC surface or porous structure interact with UV light to generate electron (e^-) and hole (h^+). The holes are trapped by H_2O or O_2 on the surface of TiO_2 particle to yield H^+ and $HO^\bullet$ radicals, which is an effective oxidation agent in destroying HAs. Generally, $HO^\bullet$ attacks the HA molecule through hydroxyl addition or hydrogen extraction effect, and HA is conversed to CO_2 and H_2O through the different paths, for example, phenols–quinones–acids–CO_2 [1]. According to Fukushima [40], the addition of $HO^\bullet$ to aromatic sites in HA yields hydroxycyclohexadienyl radicals ($HCHD^\bullet$), and further oxidation of $HCHD^\bullet$ could result in the formation of ring opened products. In addition, $HCHD^\bullet$ radicals can add to unsaturated groups in HA, such as aromatic and vinyl groups, and the resulting dialkyl peroxide is then autodegraded to $RO^\bullet$ and epoxide. The generation of CO_2 and the formation of ring-opened products may contribute to a decrease in molecular size. We may speculate that the reaction of $^\bullet OH$ radicals increased the portion of HAs with less hydrophobic and less aromatic characters. The reactions of HA with $O_2^{\bullet-}$, $HO_2^\bullet$ or $HO^\bullet$ species to generate intermediates that ultimately lead to CO_2 are depicted in the following equations. However, the molecular and structural changes during the process need further studies.

$$TiO_2 + h\nu \rightarrow h^+(VB) + e^-(CB) \tag{6}$$

$$h^+(VB) + OH^- \rightarrow HO^\bullet \tag{7}$$
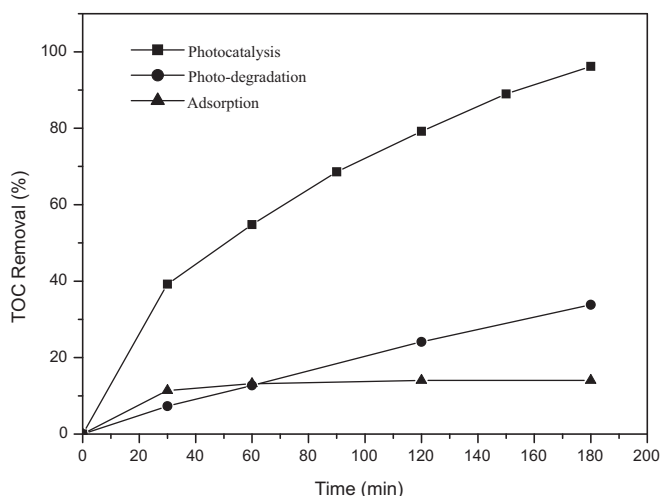
Fig. 11. Adsorption, photo- and photocatalytic degradation for HA removal.
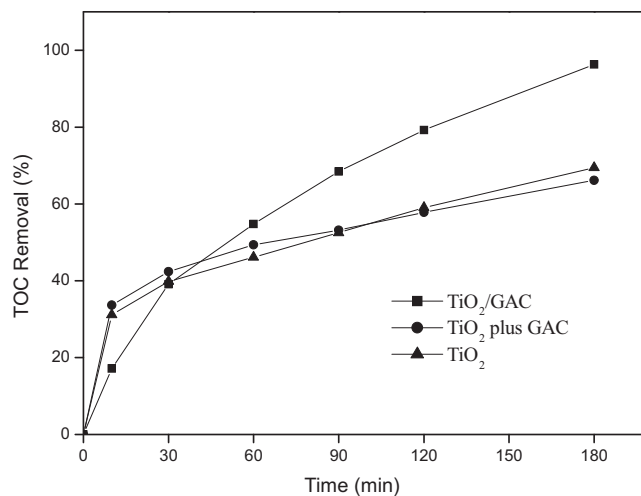
Fig. 12. Comparison of the TiO_2/GAC composite with suspended TiO_2 and suspended TiO_2 plus GAC.

$$e^-(CB) + O_2 \rightarrow O_2^{\bullet-} \tag{8}$$

$$O_2^{\bullet-} + e^-(CB) + H^+ \rightarrow H_2O_2 \tag{9}$$

$$H_2O_2 + e^-(CB) \rightarrow HO^\bullet + OH^- \tag{10}$$

$$O_2^{\bullet-} + H^+ \rightarrow HO_2 \tag{11}$$

$$HO_2^\bullet + H^+ + e^-(CB) \rightarrow HO^\bullet + OH^- \tag{12}$$

$$HA + HO^\bullet \rightarrow H_2O + CO_2 + other degradation products \tag{13}$$

$$HA + O_2^\bullet \rightarrow H_2O + CO_2 + other degradation products \tag{14}$$

$$HA + HO_2^\bullet \rightarrow H_2O + CO_2 + other degradation products \tag{15}$$

The adsorptive equilibrium was reached within 30 min, and accounted 14% of the removal of HA, whereas direct photolysis and adsorption of HA on TiO_2/GAC accounted for 40% of the amount removed.

A comparison of the degradation of HA by TiO_2/GAC, TiO_2 powders and TiO_2 plus GAC under UV radiation, is shown in Fig. 12. The weight of TiO_2 powers used in the latter two solutions was equal to that of TiO_2 in the TiO_2/GAC composite, i.e. 0.4 g/L. It can be seen that the TiO_2/GAC was the most effective and this is attributed to the synergistic effects of adsorptive properties of the GAC and photocatalytic activity of the TiO_2 in the composite. The surface adsorption of HA on the substrate enriches HA, causing a concentration effect in chemical reactions, followed by degradation intermediates on the site of the TiO_2, enhancing photocatalytic degradative activity. On the other hand, the photocatalytic reactions degrade HA and enhance HA adsorption on the surface of TiO_2/GAC. Wang et al. [29,30] also observed that the TiO_2/GAC composite exhibited a better photocatalytic performance than the mixture of TiO_2–GAC.

For the different initial concentrations of humic acid examined, the kinetics of HA degradation are presented in Fig. 13. The experimental data were fitted to the Langmuir–Hinshelwood equation, which describes the kinetics of heterogeneous catalytic chemical reactivity:

$$-\frac{dc}{dt} = \frac{K_{LH} K * C}{1 + K * C} \tag{16}$$

where C, K_{LH}, K^* are the HA concentration, Langmuir–Hinshelwood reaction rate constant and apparent adsorption constant, respectively. Based on the initial degradation rate, linearization and
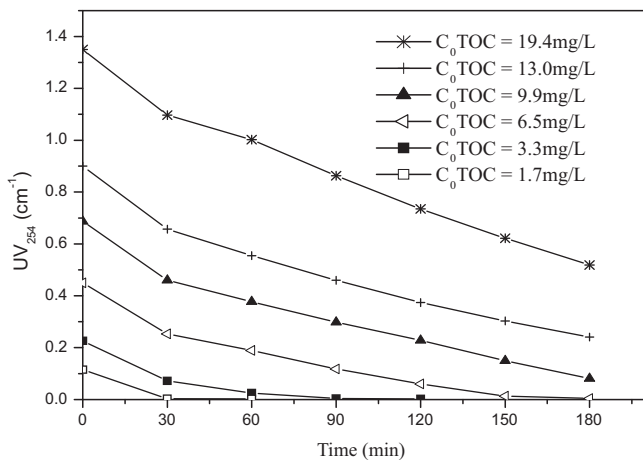
Fig. 13. The kinetics of photocatalytic degradation of humic acid at different initial concentrations.

rearrangement provides an alternate form:

$$\frac{1}{v_0} = \frac{1}{K_{LH}} + \frac{1}{K_{LH}K^*C_0} \tag{17}$$

By fitting the initial degradation rates (over the first 30 min) given in Fig. 13 into Eq. (17), we obtained the fitted parameters: $R^2 = 0.9813$, $K_{LH} = 0.1124$ mg/(L min), and $K^* = 0.3402$ L/mg. It is noted that $K^*/b = 1.7$, where b is the adsorption constant from the dark adsorption isotherms of the TiO_2/GAC photocatalyst (see Table 3). This is in agreement with the results reported by Xu and Langford (photocatalytic degradation of acetophenone over TiO_2 of Degussa P25 in aqueous medium) [41] and Minero and Vione (photocatalytic degradation of phenol over TiO_2 slurries) [42]. Xu and Langford reported that K^* decreases when the irradiation is performed at higher light intensity, whilst K_{LH} increases expectedly [41].

It should be pointed out that some photocatalysed reactions, adsorption/desorption reaction equilibria are not established during the reactions, because the substantial reactivity of an adsorbed active species (e.g., hole (h^+), radical ($OH^\bullet$), etc.) causes a continued displacement from equilibrium of the adsorbed reactant concentration. Ollis confirmed that a pseudo-steady state analysis based upon the stationary state hypothesis for reaction intermediates is consistent with the reported intensity dependence of apparent adsorption (and de-sorption) binding constants, as well as the catalytic rate constant [43].

It should also be noted that the initial time interval selected for the initial rate calculation is of critical importance in determining these final constants. This work confirmed the synergetic relationship between adsorption upon GAC and degradation involving TiO_2 in the composite material under incident UV light. Detailed kinetic models have to confront also with the complexity of charge carrier generation and migration to the catalyst surface, and interfacial electron transfer, which depends on the surface configuration.

4. Conclusions

The TiO_2/GAC composite was prepared by the sol-dipping–gel procedure and the size of TiO_2 particles supported by the GAC was calculated using Scherrer's formula to be 11.7 nm. The photocalytic activity of the TiO_2/GAC substrate was demonstrated on aqueous HA solutions, irradiated by high-intensity light with a wavelength of 365 nm. The factors influencing degradation, including TiO_2 loading and the temperature at which the composite was calcined, were investigated. The optimized TiO_2/GAC composite exhibited a high photocatalytic activity and humic acid could be rapidly removed from water. This work has highlighted the synergetic relationship between adsorption upon GAC and degradation involving TiO_2 (in the composite material) under incident UV light. Adsorption was key parameter controlling the kinetic constant of humic acid degradation, and as the surface adsorption of HA on the substrate increased, there was a consequent increase in the efficiency of degradation of HA.

References

[1] F.J. Stevenson, Humus chemistry, in: Genesis, Composition, Reactions, second ed., John Wiley & Sons, New York, 1994.
[2] R.A. Alvarez-Puebla, C. Valenzuela-Calahorro, J.J. Garrido, Theoretical study on fulvic acid structure, conformation and aggregation: a molecular modelling approach, Sci. Total Environ. 358 (2006) 243–254.
[3] N. Senesi, Aggregation patterns and macromolecular morphology of humic substances: a fractal approach, Soil Sci. 164 (1999) 841–856.
[4] N. Senesi, F.R. Rizzi, P. Dellino, P. Acquafredda, Fractal humic acids in aqueous suspensions at various concentrations, ionic strengths and pH values, Colloids Surf. A 127 (1997) 57–68.
[5] K.H. Choo, D.-I. Chang, K.-W. Park, M.-H. Kim, Use of an integrated photocatalysis/hollow fiber microfiltration system for the removal of trichloroethylene in water, J. Hazard. Mater. 152 (2008) 183–190.
[6] H. Selcuk, Disinfection and formation of disinfection by-products in a photoelectrocatalytic system, Water Res. 44 (2010) 3966–3972.
[7] R. Mosteo, N. Miguel, S. Martin-Muniesa, Maria.P. Ormad, L. José, Ovelleiro, Evaluation of trihalomethane formation potential in function of oxidation processes used during the drinking water production process, J. Hazard. Mater. 172 (2009) 661–666.
[8] O. Carp, C.L. Huisman, A. Reller, Photoinduced reactivity of titanium dioxide, Prog. Solid State Chem. 32 (2004) 33–177.
[9] S.M. Rodriguez, J.B. Galvez, M.I. Rubio, Engineering of solar photocatalytic collectors, Sol. Energy 77 (2004) 513–524.
[10] J.H. Jeon, S.D. Kim, T.H. Lim, D.H. Lee, Degradation of trichloroethylene by photocatalysis in an internally circulating slurry bubble column reactor, Chemosphere 60 (2005) 1162–1168.
[11] J. Ryu, W. Choi, K.H. Choo, A pilot-scale photocatalyst-membrane hybrid reactor: performance and characterization, Water Sci. Technol. 51 (2005) 491–497.
[12] R. Molinari, M. Borgese, E. Drioli, L. Palmisano, M. Schiavello, Hybrid processes coupling photocatalysis and membranes for degradation of organic pollutants in water, Catal. Today 75 (2002) 77–85.
[13] K. Tennakone, C.T.K. Tilakaratne, I.R.M. Kottegoda, Photocatalytic degradation of organic contaminants in water with TiO_2 supported on polythene films, J. Photochem. Photobiol. A: Chem. 87 (1995) 177–179.
[14] M.S. Lee, J.D. Lee, S.S. Hong, Photocatalytic decomposition of acetic acid over TiO_2 and TiO_2/SiO_2 thin films prepared by the sol–gel method, J. Ind. Eng. Chem. 11 (2005) 495–501.
[15] P.A. Quinlivan, L. Li, D.R.U. Knappe, Effects of activated carbon characteristics on the simultaneous adsorption of aqueous organic micro-pollutants and natural organic matter, Water Res. 39 (2005) 1663–1673.
[16] M. Nazir, J. Takasaki, H. Kumazawa, Photocatalytic degradation of gaseous ammonia and trichloroethylene over TiO_2 ultrafine powders deposited on activated carbon particles, Chem. Eng. Commun. 190 (2003) 322–333.
[17] J. Arana, J.M. Dona-Rodriguez, E.T. Rendon, TiO_2 activation by using activated carbon as a support. Part I. Surface characterization and decantability study, Appl. Catal. B: Environ. 44 (2003) 161–172.
[18] C.L. Pang, R. Lindsay, G. Thornton, Chemical reactions on rutile TiO_2 (1 1 0), Chem. Soc. Rev. 7 (2008) 2328–2353.
[19] S.K. Joung, T. Amemiya, M. Murabayashi, K. Itoh, Adsorbed species on TiO_2 associated with the photocatalytic oxidation of trichloroethylene under UV, J. Photochem. Photobiol. A: Chem. 183 (2006) 273–281.
[20] M. Munner, M. Qamar, M. Saquib, D.W. Bahnemann, Heterogeneous photocatalysed reaction of three selected pesticide derivatives, propham, propachlor and tebuthiuron in aqueous suspensions of titanium dioxide, Chemosphere 61 (2005) 457–468.
[21] J.K Yang, S.M. Lee, Removal of Cr(VI) and humic acid by using TiO_2 photocatalysis, Chemosphere 63 (2006) 1677–1684.

[22] C. Lin, K.S. Lin, Photocatalytic oxidation of toxic organohalides with TiO_2/UV: the effects of humic substances and organic mixtures, Chemosphere 66 (2007) 1872–1877.

[23] D. Dong, P. Li, X. Li, Q. Zhao, Y. Zhang, C. Jia, P. Li, Investigation on the photocatalytic degradation of pyrene on soil surfaces using nanometer anatase TiO_2 under UV irradiation, J. Hazard. Mater. 174 (2010) 859–863.

[24] A.I. Gomes, J.C. Santos, V.J.P. Vilar, R.A.R. Boaventura, Inactivation of bacteria E. coli and photodegradation of humic acids using natural sunlight, Appl. Catal. B: Environ. 88 (2009) 283–291.

[25] S. Liu, M. Lim, R. Fabris, C. Chow, K. Chiang, M. Drikas, R. Amal, Removal of humic acid using TiO_2 photocatalytic process—fractionation and molecular weight characterisation studies, Chemosphere 72 (2008) 263–271.

[26] E.S. Tsimas, K. Tyrovola, N.P. Xekoukoulotakis, N.P. Nikolaidis, E. Diamadopoulos, D. Mantzavinos, Simultaneous photocatalytic oxidation of As(III) and humic acid in aqueous TiO_2 suspensions, J. Hazard. Mater. 169 (2009) 376–385.

[27] P. Le-Clech, E.K. Lee, V. Chen, Hybrid photocatalysis/membrane treatment for surface waters containing low concentrations of natural organic matters, Water Res. 40 (2006) 323–330.

[28] S. Mozia, M. Tomaszewska, A.W. Morawski, Removal of azo-dye acid red 18 in two hybrid membrane systems employing a photodegradation process, Desalination 198 (2006) 183–190.

[29] X. Wang, Y. Liu, Z. Hu, Y. Chen, W. Liu, G. Zhao, Degradation of methyl orange by composite photocatalysts nano-TiO_2 immobilized on activated carbons of different porosities, J. Hazard. Mater. 169 (2009) 1061–1067.

[30] X. Wang, Z. Hu, Y. Chen, G. Zhao, Y. Liu, Z. Wen, A novel approach towards high-performance composite photocatalyst of TiO_2 deposited on activated carbon, Appl. Surf. Sci. 255 (2009) 3953–3958.

[31] H.T.T. Kiyonaga, S.I. Naya, Rational design and applications of highly efficient reaction systems photocatalyzed by noble metal nanoparticle-loaded titanium(IV) dioxide, Chem. Soc. Rev. 38 (2009) 1849–1858.

[32] R. Al-Rasheed, D.J. Cardin, Photocatalytic degradation of humic acid in saline waters. Part 1. Artificial seawater: influence of TiO_2, temperature, pH, and airflow, Chemosphere 51 (2003) 925–933.

[33] M. Bekbolet, A.S. Suphandag, C.S. Uyguner, An investigation of the photocatalytic efficiencies of TiO_2 powders on the decolorisation of humic acids, J. Photochem. Photobiol. A: Chem. 148 (2002) 121–128.

[34] T.W. Zerda, X. Yuan, S.M. Moore, C.A.L. Leon, Surface area, pore size distribution and microstructure of combustion engine deposits, Carbon 37 (1999) 1999–2009.

[35] J.P Pinheiroa, A.M. Mota, J.M.R. d'Oliveira, J.M.G. Martinho, Dynamic properties of humic matter by dynamic light scattering and voltammetry, Anal. Chim. Acta 329 (1996) 15–24.

[36] M.M. Yee, T. Miyajima, N. Takisawa, Study of ionic surfactants binding to humic acid and fulvic acid by potentiometric titration and dynamic light scattering, Colloids Surf. A: Physicochem. Eng. Aspects 347 (2009) 128–132.

[37] H.K. Powell, R.M. Town, Solubility and fractionation of humic acid: effect of pH and ionic medium, Anal. Chim. Acta 267 (1992) 47–54.

[38] M.S. Shevchenko, G.W. Bailey, L.G. Akim, The conformational dynamics of humic polyanions in model organic and organo-mineral aggregates, J. Mol. Struct. (Theochem.) 460 (1999) 179–190.

[39] R. Baigorri, M. Fuentes, G. Gonzalez-Gaitano, J.M. Garcia-Mina, Analysis of molecular aggregation in humic substances in solution, Colloids Surf. A: Physicochem. Eng. Aspects 302 (2007) 301–306.

[40] M. Fukushima, K. Tatsumi, S. Nagao, Degradation characteristics of humic acid during photo-Fenton processes, Environ. Sci. Technol. 35 (2001) 3683–3690.

[41] Y.M. Xu, C.H. Langford, Variation of Langmuir adsorption constant determined for TiO_2-photocatalyzed degradation of acetophenone under different light intensity, J. Photochem. Photobiol. A: Chem. 133 (2000) 67–71.

[42] C. Minero, D. Vione, A quantitative evaluation of the photocatalytic performance of TiO_2 slurries, Appl. Catal. B: Environ. 67 (2006) 257–269.

[43] D.F. Ollis, Kinetics of liquid phase photocatalyzed reactions: an illuminating approach, J. Phys. Chem. B 109 (2005) 2439–2444.